

Accelerating Barnes-Hut t-SNE Algorithm by Efficient Parallelization on Multi-Core CPUs

Narendra Chaudhary, Alexander Pivovar, Pavel Yakovlev, Andrey Gorshkov,
Sanchit Misra

[narendra.chaudhary,alexander.pivovar,pavel.yakovlev,andrey.gorshkov,sanchit.misra]@intel.com
Intel Corporation

ABSTRACT

t-SNE remains one of the most popular embedding techniques for visualizing high-dimensional data. Most standard packages of t-SNE, such as scikit-learn, use the Barnes-Hut t-SNE (BH t-SNE) algorithm for large datasets. However, existing CPU implementations of this algorithm are inefficient. In this work, we accelerate the BH t-SNE on CPUs via cache optimizations, SIMD, parallelizing sequential steps, and improving parallelization of multithreaded steps. Our implementation (Acc-t-SNE) is up to 261× and 4× faster than scikit-learn and the state-of-the-art BH t-SNE implementation from daal4py, respectively, on a 32-core Intel®Icelake cloud instance.

Project Code URL: https://github.com/IntelLabs/TransOmics-Acceleration-Library/tree/master/applications/single_cell_pipeline

KEYWORDS

Machine Learning, High Performance Computing, Genomics, Data Visualization, Efficient Hardware Optimization

ACM Reference Format:

Narendra Chaudhary, Alexander Pivovar, Pavel Yakovlev, Andrey Gorshkov, Sanchit Misra. 2022. Accelerating Barnes-Hut t-SNE Algorithm by Efficient Parallelization on Multi-Core CPUs. In *Proceedings of* . ACM, New York, NY, USA, 13 pages. <https://doi.org/10.1145/nnnnnnn.nnnnnnn>

1 INTRODUCTION

Data analysis is the first step in many machine learning applications, and data visualization is a core component of data analysis. Visualization of complex high-dimensional data provides insights for hypothesis formation, algorithm choice, and hardware selection. Visualization techniques can also provide valuable insights into the inner workings of deep learning algorithms. Additionally, visualization techniques such as t-SNE [21] and UMAP [14] have found applications in large scale genomics data analysis. For example, t-SNE is used to visualize proximal cells in high-dimensional single-cell RNA-seq data [1].

We can visualize a set of high-dimensional data points in two or three dimensions by using a dimensionality reduction technique. Dimensionality reduction techniques can be

broadly classified into linear and non-linear techniques. Linear techniques, such as Principal Component Analysis (PCA), focus on keeping the low-dimensional representations of far-apart points. Alternately, non-linear dimensionality reduction techniques, such as the t-SNE, focus on local distances and use neighborhood graphs to construct low-dimensional embeddings.

Exact computation of t-SNE embeddings [21] can be very slow. Therefore, Maaten et. al., [20] proposed t-SNE acceleration using the tree-based Barnes-Hut[2] algorithm for computation of repulsive forces. Scikit-learn [18], Multicore-TSNE [19], and daal4py [7] provide parallel implementations of this algorithm for CPUs. Both Multicore-TSNE and daal4py t-SNE implementations are faster than scikit-learn for large datasets. To the best of our knowledge, daal4py t-SNE is the fastest implementation of BH t-SNE for CPUs. Fit-SNE [13] uses an FFT-interpolation-based approach to compute further approximation of the repulsive force. Fit-SNE can be significantly faster, especially for large datasets. In addition to CPU implementations, there are several GPU accelerated t-SNE implementations [3, 5, 6, 17]. These approaches attempt to implement efficient GPU versions of BH t-SNE and Fit-SNE.

1.1 Our Contributions

In this work, we start with the existing daal4py implementation of BH t-SNE consisting of the following major steps: (1) K Nearest Neighbors (KNN), (2) Binary Search Perplexity (BSP), (3) Quadtree building, (4) Summarization, (5) Attractive force computation, and (6) Repulsive force computation. KNN implementation in daal4py is already fairly efficient. We speedup the other steps on CPUs as follows.

- (1) We adopt a Morton-code based algorithm to make quadtree building more efficient and parallelization friendly. Additionally, we develop a vectorized (SIMD) and multithreaded version of the quadtree building algorithm that scales significantly better than daal4py.
- (2) Morton code based quadtrees, along with our efficient data layout, also improve single-thread performance of Summarization and Repulsive force computations.

- (3) We apply SIMD parallelism and software prefetching to the attractive force computation to improve the single-thread performance and multithread scaling.
- (4) We accelerate the existing sequential implementations of BSP and Summarization by multithreading.

Our single-thread improvements provide up to $2.6\times$ speedup over daal4py t-SNE. On a 32-core Intel®IceLake based cloud instance, our implementation (Acc-t-SNE) achieves up to $21\times$ speedup over single-threaded execution. This combination of improvements in single-thread performance and multi-thread scaling achieves up to $4\times$ speedup over state-of-the-art BH t-SNE implementation – daal4py. Additionally, Acc-t-SNE is up to $29\times$ faster than Multicore-TSNE, up to $3.8\times$ faster than Flt-SNE, and up to $261\times$ faster than scikit-learn t-SNE.

2 BACKGROUND

2.1 Problem Statement

Given the high dimensional input dataset $X = \{x_1, x_2, \dots, x_N\}$ containing N high-dimensional points x_i , we want to reduce it to two or three-dimensional embedding $Y = \{y_1, y_2, \dots, y_N\}$ so that it can easily be visualized in a scatterplot. The goal is to preserve as much of the significant structure of the high-dimensional data as possible in the low-dimensional map. For brevity, we only discuss the case with a two-dimensional Y in this paper as it is the most common use case.

2.2 Brief overview of the Barnes Hut t-SNE Algorithm

The t-distributed Stochastic Neighbor Embedding (t-SNE), first proposed by [20, 21], is based on the Stochastic Neighbor Embedding (SNE) [9] technique for data visualization and dimensionality reduction. It starts by converting the high-dimensional distances between all pairs of data points (x_i, x_j) into joint probabilities (p_{ij}) that represent similarities. Subsequently, it randomly initializes corresponding points in the low dimensional space and calculates joint probabilities (q_{ij}) between all pairs of data points (y_i, y_j). The algorithm aims to find the embeddings of the low dimensional points, such that the difference between p_{ij} and q_{ij} is minimized. The t-SNE algorithm consists of the following steps:

2.2.1 Input similarity computation. In the first step, the algorithm computes similarities (p_{ij}) between high-dimensional input point pairs (x_i, x_j) based upon distance between them (d_{ij}) using Gaussian kernels.

$$p_{j|i} = \frac{\exp(-d_{ij}^2/2\sigma_i^2)}{\sum_{k \neq i} \exp(-d_{ik}^2/2\sigma_i^2)}, \quad p_{i|i} = 0 \quad (1)$$

$$p_{ij} = \frac{p_{i|j} + p_{j|i}}{2N}$$

Here, σ_i is the variance of the Gaussian kernel that is centered on data point x_i . These variances are set based upon a predefined input parameter called perplexity, denoted here by u . Values of σ_i^2 vary per object, and σ_i^2 tend to have smaller values in higher data density regions. The similarities (p_{ij}) form a joint probability distribution over all point pairs (x_i, x_j), and can be represented as an $N \times N$ similarity matrix P .

Similarities (p_{ij}) for distant points i and j can be extremely small. Therefore, [20] proposed a sparse approximation of the similarity matrix (P). Sparse approximation accelerates the t-SNE algorithm without impacting the quality of the low dimension embedding. The algorithm obtains the sparse approximation by first finding $\lfloor 3u \rfloor$ nearest neighbors of each input point and then redefining the input similarities as following:

$$p_{j|i} = \begin{cases} \frac{\exp(-d_{ij}^2/2\sigma_i^2)}{\sum_{k \in N_i} \exp(-d_{ik}^2/2\sigma_i^2)}, & \text{if } j \in N_i \\ 0, & \text{otherwise} \end{cases} \quad (2)$$

$$p_{ij} = \frac{p_{i|j} + p_{j|i}}{2N}$$

Here, N_i are $\lfloor 3u \rfloor$ neighborhood points of x_i . Values of σ_i^2 are set such that the perplexity of the conditional distribution is equal to input perplexity u via a binary search over σ_i^2 . The nearest neighbors are found via the **k-nearest neighbors (KNN)** step and σ_i^2 by **binary search perplexity (BSP)** step.

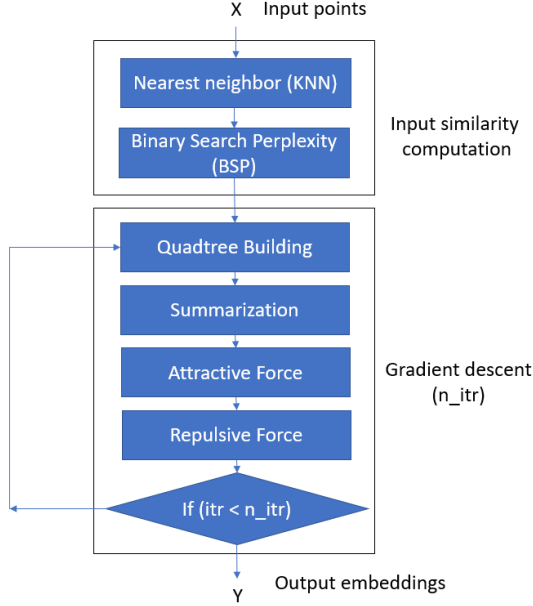
Similarities q_{ij} also get computed for low-dimensional embedding points Y . Here, the t-SNE algorithm uses the normalized Student-t kernel with a single degree of freedom to compute embedding space similarities q_{ij} .

$$q_{ij} = \frac{(1 + \|y_i - y_j\|^2)^{-1}}{\sum_{k \neq i} (1 + \|y_k - y_i\|^2)^{-1}}, \quad q_{ii} = 0 \quad (3)$$

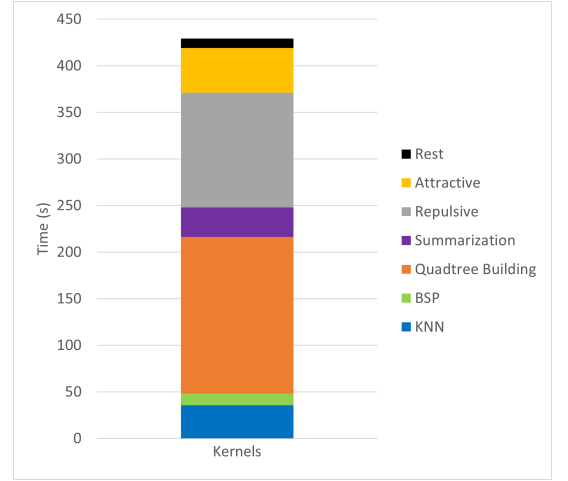
Similarities in embedding space q_{ij} also form a joint-probability distribution over all embedding point pairs (y_i, y_j), and can be represented as an $N \times N$ similarity matrix Q .

2.2.2 Gradient Descent. As a metric of difference between all the p_{ij} and q_{ij} values, t-SNE uses **Kulback-Leibler divergence (KL divergence)** since it helps to preserve the local structure of points. Therefore, minimizing the difference between p_{ij} and q_{ij} is the same as minimizing the KL divergence between the probability distributions of high-dimensional input space (P) and low-dimensional embedding space (Q). The algorithm uses gradient descent to minimize the KL divergence cost C .

$$C(y) = KL(P||Q) = \sum_{i \neq j} p_{ij} \log \frac{p_{ij}}{q_{ij}} \quad (4)$$



(a) Major Steps of the BH t-SNE algorithm.



(b) Profile of the BH t-SNE algorithm based implementation in daal4py v.2021.6 with a dataset of 1 million cells subsampled from the mouse brain cell dataset described in Section 4.2

Figure 1: The BH t-SNE algorithm and its profile.

By taking the gradient of the cost with respect to y_i ,

$$\frac{\partial C}{\partial y_i} = 4 \sum_{i \neq j} (p_{ij} - q_{ij}) q_{ij} Z(y_i - y_j) \quad (5)$$

Where, $Z = \sum_{k \neq l} (1 + \|y_k - y_l\|^2)^{-1}$ is a normalization term. The cost gradient can be split into two parts,

$$\frac{\partial C}{\partial y_i} = 4 \left(\sum_{i \neq j} p_{ij} q_{ij} Z(y_i - y_j) - \sum_{i \neq j} q_{ij}^2 Z(y_i - y_j) \right) \quad (6)$$

Here, the first summation can be interpreted as the attractive force F_{attr} from all points on y_i , and the second summation can be interpreted as the repulsive force F_{rep} from all points.

$$\frac{\partial C}{\partial y_i} = 4(F_{attr} + F_{rep}) \quad (7)$$

Attractive Force Computation: By recognising, $q_{ij} Z(y_i - y_j) = (1 + \|y_i - y_j\|^2)^{-1}$,

$$F_{attr} = \sum_{i \neq j} \frac{p_{ij}}{(1 + \|y_i - y_j\|^2)} \quad (8)$$

. Therefore, attractive force computation a y_i point can be done by performing the above summation over all non-zero elements from i_{th} row of the sparse matrix P .

Repulsive Force Computation: The exact computation of all repulsive forces F_{rep} has $O(N^2)$ computational complexity.

Therefore, doing it at every gradient descent step is expensive.

Maaten et. al. [20] proposed accelerating the t-SNE repulsive force computation to $O(N \log(N))$ time complexity by doing an approximate computation of F_{rep} using the **Barnes-Hut algorithm** [2]. The Barnes-Hut method leverages the insight that, for any point, points that are distant in low dimensional space and are close to each other, exert nearly the same force. This method has three steps, 1) **Quadtree building** from current Y , 2) **Summarization** and 3) **Repulsive Force** computation via Quadtree traversal in $O(N \log(N))$ time. We provide more details of these steps in Section 3.3.

In summary, Figure 1a illustrates the major steps of the BH t-SNE algorithm – 1) K-nearest neighbors (KNN), 2) Binary Search Perplexity (BSP), and for each iteration of gradient descent – 3) Quadtree building, 4) Summarization, 5) Attractive force computation, and 6) Repulsive force computation.

2.3 Profile of BH t-SNE algorithm

We use daal4py [7] implementation of BH t-SNE for profiling since, based on our experiments, that is the fastest implementation prior to our work. We obtain the profile on a 32-core CPU described in Table 2 using one of the largest datasets described in Section 4.2. Figure 1b shows that BH t-SNE has a relatively flat profile, thus requiring acceleration of all the steps in order to achieve end-to-end acceleration.

Table 1: Summary of improvements in each step.

STEP	IMPROVEMENTS
BSP	MULTITHREADING WITH NUMBA
QUADTREE BUILDING	MORTON CODES TO MAKE PARALLELIZATION FRIENDLY, MULTITHREADING, DATA LAYOUT IMPROVEMENTS
SUMMARIZATION	MULTITHREADING
REPULSIVE	DATA LAYOUT IMPROVEMENT
ATTRACTIVE	SIMD, SOFTWARE PREFETCHING

3 OUR ACCELERATION OF BH T-SNE

We use the implementation of BH t-SNE in daal4py [7] v.2021.6.0 as our baseline implementation and build our accelerated implementation on top of that. Given the flat profile, we accelerate most of the major steps of the algorithm (shown in Figure 1a) with additional emphasis on steps that are more time consuming. For example, since BSP takes a very small percentage of the time, we accelerate it by multi-threading the existing Python source code in daal4py using Numba [11]. On the other hand, steps such as quadtree building, attractive force computation, repulsive force computation, consume large percentages of time. For these steps, we worked on the existing C++ implementation under daal4py and used rigorous methods such as 1) modifying the algorithm to make it more parallelization friendly, 2) data layout changes to improve data locality, 3) multi-threading, 4) software prefetching to alleviate memory latency bottleneck and 4) SIMD to reduce number of instructions. We provide a summary of our improvements to each step in Table 1 and more details in the following Subsections.

3.1 K Nearest Neighbours

We use the existing KNN implementation from daal4py for our optimized code. Daal4py version of KNN is fairly efficient and scales well with the number of cores as shown in Section 4.6 and Figure 6a.

3.2 Binary Search Perplexity

This step computes the conditional similarities $p_{j|i}$ for all input point pairs based upon equation 2. For each i , it computes the equation 2 multiple times with different values of σ_i^2 until the perplexity of the conditional distribution $p_{j|i}$ is equal to input target perplexity u . This search for the value of σ_i^2 is performed through a binary search where in each step, σ_i^2 is the middle point of successively smaller intervals. Prior implementations of this BSP are single-threaded. We have parallelized this step by recognizing that we can compute

$p_{j|i}$ for each i independently in parallel. We use Numba’s [11] parallel range utility to multi-thread this step.

3.3 Quadtree Building

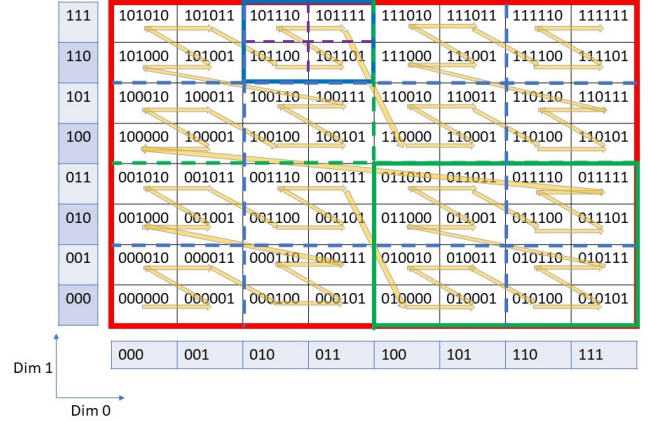


Figure 2: Two-dimensional space split into hierarchical cells. Binary numbers are Morton codes associated with cells. The increasing order of morton code follows the orange line (Z-order).

At every gradient step of the BH t-SNE algorithm, we need to build a new quadtree to compute repulsive forces F_{rep} . The boundaries of the output two-dimensional space are defined by the minimum/maximum values in Y along the two dimensions. The BH method partitions this two-dimensional space into four quadrants creating four rectangular cell. These cells are recursively partitioned into four sub quadrants each creating smaller cells until 1) there is only a single point in a cell or 1) the cells are too small. The root node of the quadtree represents the entire two-dimensional space. Each non-leaf node represents a rectangular cell of the two-dimensional space and has four children corresponding to its four sub-quadrants. Leaf nodes represent a cell containing a single point. Figure 2 shows a two-dimensional space partitioned into cells, and Figure 3 shows the quadtree associated with those cells. For illustration, we color some cells in Figure 2 and corresponding nodes in Figure 3 to show the relationship.

Daal4py constructs the quadtree by going through the various levels of the tree starting from the root level. At each level, it goes through each node of the tree and checks for the corresponding cell needs to be partitioned into quadrants. If a cell needs partitioning, it creates four children of the corresponding node and divides all the points in that cell into the four quadrants. This algorithm is computationally very expensive since each time a cell is partitioned, we need to go over all the points in the cell to split them across the

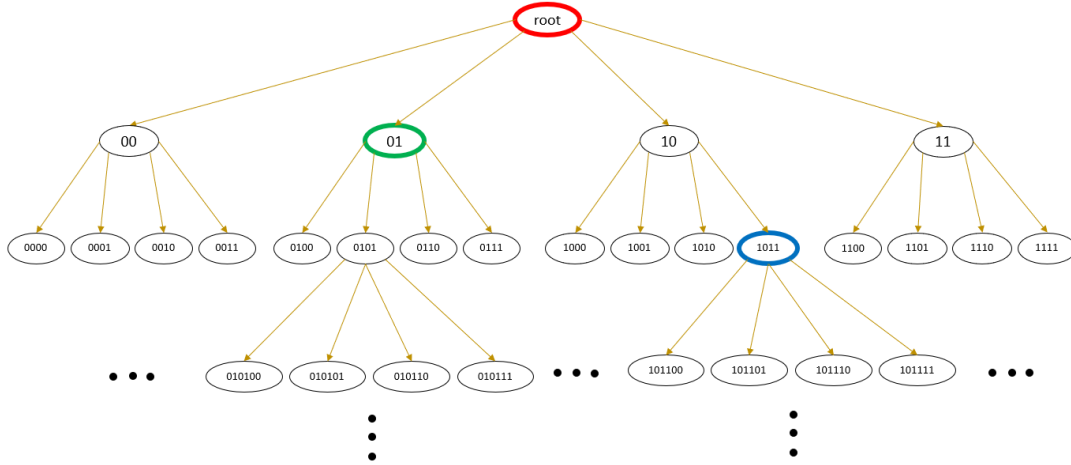


Figure 3: Quadtree representation of two-dimensional space. Each non-leaf node represents a cell. Binary numbers are Morton codes associated with cells.

quadrants. So, each point is traversed as many times as the depth of the tree for that point. Instead, similar to [3], we use Morton codes that allows us to traverse each point only once. Morton codes are also useful for making the algorithm more parallelization friendly.

Morton Codes: Morton codes [15] are spatial location codes [22] that map multi-dimensional data into one-dimension while preserving the locality of data points. We form Morton codes by bitwise interleaving of the coordinates in the two dimensions. For example, dimension 0 value of $3 = 011_b$ and dimension 1 value of $7 = 111_b$ has Morton code of $47 = 101111_b$ (see Figure 2).

Morton codes or Z-order codes have several properties due to which they are used in quadtree construction [22]. In general, they are used in construction of bounded volume hierarchies [12]. Sorted Morton codes ensure that the data points that are clustered close to each other in two-dimension are also close to each other in the sorted order. Therefore, they get stored close together in a one-dimensional data structure. Additionally, a quadtree cell/node can be represented as a linear range of Morton codes. For example, in Figure 2 the blue colored cell can be represented as a range $\{101100_b, \dots, 101111_b\}$ and the green colored cell can be represented as a range $\{010000_b, \dots, 011111_b\}$. The longest common prefix of the Morton codes in a cell is enough to identify tree level and cell (see Figure 3). Depth-first traversal can also be understood as selecting subranges recursively from the full range of Morton codes. We use 64-bit Morton codes that can represent 2^{64} cells. First, we convert each two-dimensional point into a Morton code by using Algorithm 1. The algorithm computes Morton codes from maximum span radius (r_{span}) of 2D space and its center point ($cent[0], cent[1]$). We can construct each embedding point's

Algorithm 1 Morton Code Formation Algorithm

- 1: **Input:** Embedding points $y_i = (y_i[0], y_i[1]), \forall i \in \{0, N-1\}$, $(cent[0], cent[1]), r_{span}$
 - 2: **Output:** 64-bit Morton codes $M_i, \forall i \in \{0, N-1\}$
 - 3: Initialize $M_i = 0, \forall i \in \{0, N-1\}$.
 - 4: $(y_{root}[0], y_{root}[1]) \leftarrow (cent[0] - r_{span}, cent[1] - r_{span})$
 - 5: $scale = 2^{31}/r_{span}$
 - 6: **for** $i = 0$ **to** $N-1$ **in parallel do**
 - 7: $(m[0], m[1]) \leftarrow (y_i[0] - y_{root}[0], y_i[1] - y_{root}[1]) * scale$
 - 8: **for** $d = 0$ **to** 1 **do**
 - 9: $m[d] \leftarrow m[d] \text{ and } (0 \times 00000000 \text{ ffffffff})$
 - 10: $m[d] \leftarrow m[d] \text{ or } (m[d] \ll 16)$
 - 11: $m[d] \leftarrow m[d] \text{ and } (0 \times 0000 \text{ ffff} 0000 \text{ ffff})$
 - 12: $m[d] \leftarrow m[d] \text{ or } (m[d] \ll 8)$
 - 13: $m[d] \leftarrow m[d] \text{ and } (0 \times 00 \text{ ff} 00 \text{ ff} 00 \text{ ff} 00 \text{ ff})$
 - 14: $m[d] \leftarrow m[d] \text{ or } (m[d] \ll 4)$
 - 15: $m[d] \leftarrow m[d] \text{ and } (0 \times 0 \text{ f} 0 \text{ f})$
 - 16: $m[d] \leftarrow m[d] \text{ or } (m[d] \ll 2)$
 - 17: $m[d] \leftarrow m[d] \text{ and } (0 \times 3333333333333333)$
 - 18: $m[d] \leftarrow m[d] \text{ or } (m[d] \ll 1)$
 - 19: $m[d] \leftarrow m[d] \text{ and } (0 \times 5555555555555555)$
 - 20: **end for**
 - 21: $M_i \leftarrow m[0] \text{ or } (m[1] \ll 1)$
 - 22: **end for**
-

Morton code independently. Therefore, codes or all N embedding points can be constructed in parallel. We use both SIMD parallelism – automatically done by the compiler due

to the simple structure of the algorithm – and explicit multi-threading.

Parallel Quadtree Building: At any level of the tree, all the nodes and the subtrees rooted at those nodes can be processed in parallel. One way to parallelize quadtree building is to distribute the nodes at each level across threads. However, many levels near the top and bottom of the tree may not have sufficient nodes to keep all the threads busy. Moreover, nodes created by a thread may be processed for further partitioning in the next level by another thread hampering data locality and causing data to jump from cache of one core to another. Therefore, we use a different approach. First, we create the tree to the minimum level such that there are sufficiently large number of nodes at that level. Subsequently, we distribute the nodes at that level across threads. Each thread is responsible not only for processing the assigned nodes but also creating the entire subtrees rooted at those nodes. Since different subtrees may be of different sizes – thus requiring different amount of work, we use dynamic thread scheduling over the nodes. For dynamic thread scheduling, the number of nodes need to be sufficiently larger than the number of threads. We also store all the nodes of a tree at a particular level in a contiguous manner to aid data locality.

3.4 Parallel Summarization

After the quadtree is built, the summarization step computes the center-of-mass for each cell in the constructed quadtree for future use in the repulsion step. The current daal4py implementation of the summarization step is single-threaded, and therefore it can take a significant amount of time for large-scale datasets (see Figure 1b). In the summarization step, we traverse the quadtree from the bottom up to compute the center-of-mass of all cells. For leaf nodes, the mass is always one. For non-leaf nodes, the center-of-mass gets computed based on the number of points and their positions inside the cell. To compute the center-of-mass of a higher-level node, we only need the center-of-mass of its four children and the count of points in them. Therefore, we can compute the center-of-mass of all the cells at one level of the quadtree in parallel. Hence, we start from the bottom level, processing all the nodes in parallel, and then proceed to the level above it.

3.5 Repulsive Force Computation

While computing F_{rep} for a point, if a cell is sufficiently far and sufficiently small, BH method approximates the contribution of all the points in the cell with the summary of the cell. To compute repulsive force on a point, the BH method traverses the quadtree in a depth-first search (DFS) manner. At each node of the tree, it checks if the summary at the node can be used as approximation instead of going further down

Algorithm 2 Attractive force algorithm in daal4py

```

1: Input: Embedding points  $y_i = (y_i[0], y_i[1]), \forall i \in \{0, N - 1\}$ , Sparse similarity CSR matrix  $P = (row, col, val)$ 
2: Output:  $F_{attr} = (attr_i[0], attr_i[1]), \forall i \in \{0, N - 1\}$ 
3: for  $i = 0$  to  $(N - 1)$  in parallel do
4:    $(attr_i[0], attr_i[1]) \leftarrow (0, 0)$ 
5:   for  $ind = row[i]$  to  $(row[i + 1] - 1)$  do
6:      $j \leftarrow col[ind] - 1$ 
7:      $PQ \leftarrow \frac{val[ind]}{(1+(y_i[0]-y_j[0])^2+(y_i[1]-y_j[1])^2)}$ 
8:      $attr_i[0] \leftarrow attr_i[0] + PQ * (y_i[0] - y_j[0])$ 
9:      $attr_i[1] \leftarrow attr_i[1] + PQ * (y_i[1] - y_j[1])$ 
10:  end for
11: end for

```

the subtree. The summary is used if the following condition, proposed by [2], is true:

$$\frac{r_{cell}}{\|y_i - y_{cell}\|^2} < \theta \quad (9)$$

Where $\|y_i - y_{cell}\|^2$ is the square of the distance to the cell, r_{cell} is the radius of the cell and θ is an input parameter that trades off speed and accuracy.

The DFS of the tree can lead to irregular memory access leading to memory latency bottlenecks if the nodes of the tree are randomly located. However, due to the structured data locality of our quadtree, the DFS experiences significantly better data locality, thereby accelerating the repulsive step.

3.6 Attractive Force Computation

Equation 8 computes the attractive force on a embedding point y_i by all other points y_j . The input similarities p_{ij} are computed only once, before the start of gradient descent steps. In approximate similarity computation [20] the similarities p_{ij} are only calculated for set of $[3u]$ nearest neighbors N_i of each input N . Therefore, the similarity matrix, P is a sparse matrix with few non-zero values and is stored in compressed sparse row (CSR) format. The calculation of F_{attr} for each y_i – equivalent to processing the i -th row of the CSR matrix – is independent and can be done in parallel. The daal4py implementation of Algorithm 2 takes this approach and scales well to multiple cores, as shown in Figure 6a. Therefore, we focus on improving the single-threaded performance of the attractive step. We can observe from the innermost for loop of Algorithm 2 that, for each y_i , all its neighbors y_j are read. There are $[3u]$ such y_j values spread over an array of N points in a pseudo random fashion. Given $[3u] \ll N$, accessing y_j could lead to irregular memory accesses. This can cause misses in caches of different levels depending upon the size of N . Larger values of N will cause more cache misses causing CPU stalls. We alleviate this by

Table 2: System Configuration.

	AWS EC2 C6i.16XLARGE
CORES / CPU	32
THREADS / CORE	2
AVX REGISTER WIDTH (BITS)	512, 256, 128
VECTOR PROCESSING UNITS (VPU)	2/CORE
BASE CLOCK FREQUENCY (GHz)	2.9
L1D, L2 CACHE (MiB)	1.5, 40
L3 CACHE (MiB) / CPU	54
DRAM (GiB) / CPU	256

software prefetching the y_j values of a later y_i while we are processing the current y_i . Better cache locality also result in better multithread scaling.

In addition to software prefetching, we also improve the single-threaded performance via SIMD parallelization of the innermost loop. Since the datatype is double-precision floating point, we hand-vectorize the innermost loop with AVX512 to process eight loop iterations simultaneously. We use AVX512 instructions for load, store and several compute operations. We also need to use AVX512 gather operation for gathering eight y_i values. There is sufficient compute in the innermost loop so that, despite the high latency of gather operations, we see healthy performance improvement due to vectorization.

4 EXPERIMENTS AND RESULTS

In this section, we first detail our experimental setup and datasets used. Subsequently, we present results on comparison of end-to-end execution time and accuracy of our implementation with other implementations. Our results show that we achieve significant performance gain without compromising accuracy. Further, we deep dive into the various dimensions of performance improvement - single thread performance and multicore scaling - for end-to-end execution and individual steps.

4.1 Experimental setup

All of the experiments presented in this paper are conducted on AWS EC2 c6i.16xlarge cloud instances as briefed in Table 2. The instance provides a 32 core 3rd generation Intel® Xeon® Platinum 8375C @2.90 GHz base clock frequency and 256 GB memory over a single NUMA domain. For more details, visit [4]. All the experiments use a single thread per core. Following the evaluation methodology used in [20], we run each implementation for 1000 iterations. Additionally, we keep input parameter values same as the default parameters of scikit-learn t-SNE.

4.2 Datasets

We conduct experiments with six datasets of different types, sizes, and input dimensions. These standard datasets are readily obtainable from internet for experimentation.

Mouse brain cell dataset: The mouse brain cell dataset [1] contains single-cell RNA sequencing (scRNA-seq) data for 1.3 million mouse brain cells. The original raw dataset contains 27998 features for each cell. However, in a single-cell pipeline, t-SNE usually gets computed after data preprocessing and principal component analysis (PCA) steps. We run the t-SNE algorithm after PCA, with 20 principal components as features. The final dataset contains 1291337 data points, each with 20 features or dimensions.

Digit dataset: The Digit dataset from scikit-learn [18] contains 1797 grayscale images of size $8 \times 8 = 64$ pixels. Each image contains a handwritten digit between $\{0, 1, \dots, 9\}$.

MNIST dataset: The MNIST handwritten digits dataset [8] contains 70000 grayscale images of size $28 \times 28 = 784$ pixels.

CIFAR10 dataset: The CIFAR-10 dataset [10] contains 60000 color images of size 32×32 pixels. The dataset consists of images of ten different classes or objects. The dataset has 3072 ($32 \times 32 \times 3$) features or input dimensions.

Fashion MNIST dataset: The fashion MNIST dataset [23] contains 70000 grayscale images of size $28 \times 28 = 784$ pixels. The dataset contains images of fashion products from 10 different categories.

SVHN dataset: The street view house numbers (SVHN) dataset [16], we use contains 99289 color images of size 32×32 pixels. The dataset contains google street view images of house numbers and has ten different classes.

Except the mouse brain cell dataset, we apply t-SNE algorithm directly on input points and collect execution time and divergence results. Supplementary Figures S1, S2, S3, S4, S5, and S6 show the visualization plots for these datasets with different t-SNE implementations.

4.3 Comparison of end-to-end performance with state-of-the-art

In this section, we compare the end-to-end execution time of Acc-t-SNE for several standard datasets with the state of the art implementations: scikit-learn t-SNE (Sklearn) [18], multicore t-SNE (Multicore) [19], FFT-accelerated Interpolation-based t-SNE (FIT-SNE) [13] and the t-SNE implementation in daal4py v2021.6.0 [7]. We run all of these algorithm in double-precision (float64) data format for consistency and fair comparison.

Figure 4 presents the comparison. Since the implementation in scikit-learn is the most widely used, we present the speedup of various implementations over that. Acc-t-SNE is consistently the fastest, achieving speedups of $5.4 \times -261.2 \times$

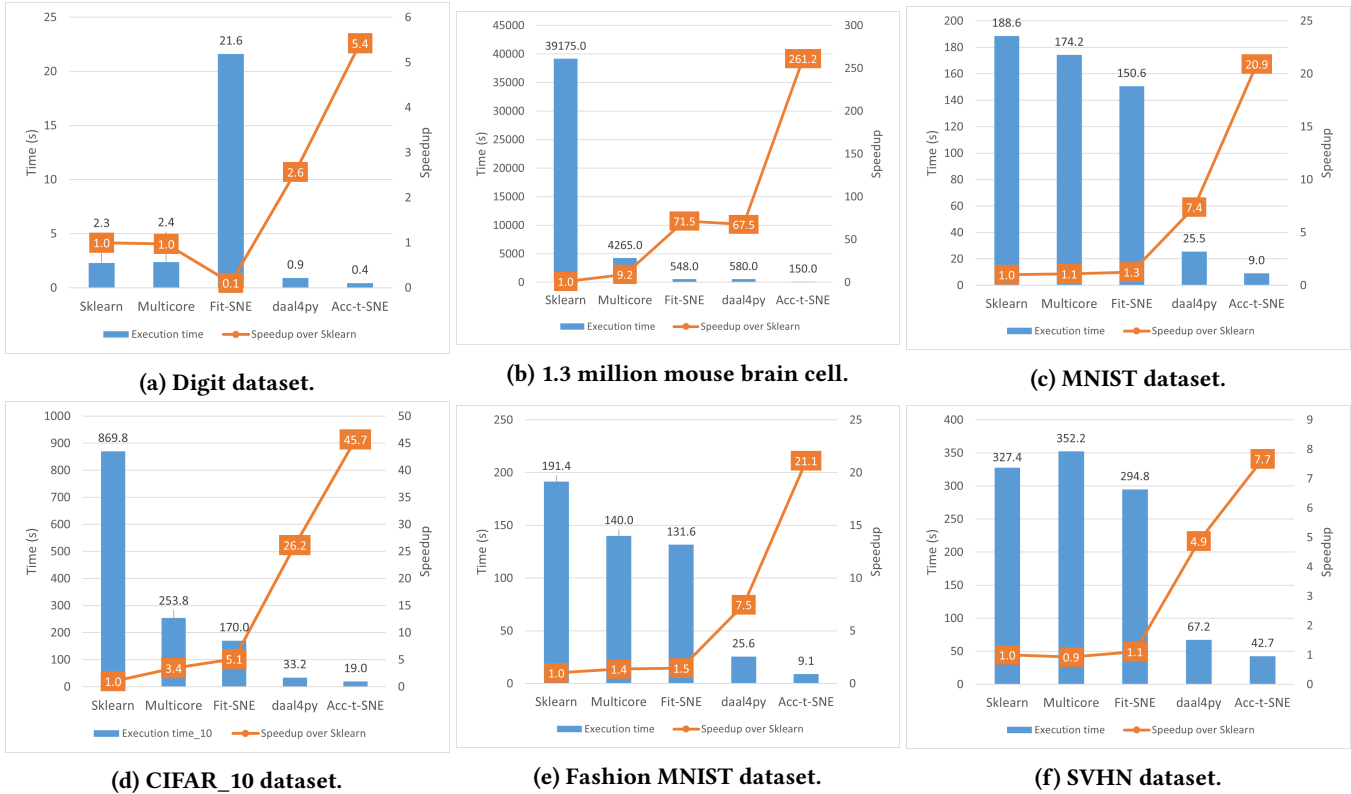


Figure 4: End-to-end performance comparison of the various implementations using all 32 cores over six standard datasets. The bars represent the execution time for each implementation, while the line represents the speedup of each implementation over Sklearn.

over scikit-learn. Speedup on a particular dataset depends on a variety of factors such as dataset size, input dimension size, etc. In general, larger datasets have more opportunity of parallelism due to wider quadrees, and therefore, the speedup is higher for larger datasets. Additionally, we can also run the Acc-t-SNE implementation in single-precision (float32) data format and achieve upto 1.6 \times speedup over the double-precision implementation without significant loss of accuracy (see Supplementary Table S1).

4.4 Evaluation of accuracy

In this section, we evaluate the accuracy of Acc-t-SNE. We compared our accuracy against two implementations: 1) scikit-learn, since it is the most widely used, and 2) daal4py, since Figure 4 shows that it is the fastest implementation prior to our work. We use the standard metric of accuracy comparison - KL-divergence that measures the difference between probability distributions of the input space and the embedding space. As can be seen from Table 3, the KL-divergence values of Acc-t-SNE are very close to the smallest

Table 3: Comparison of accuracy for all the six datasets. The lowest KL-divergence values for each dataset are highlighted in bold font.

DATASET	SKLEARN	DAAL4PY	OPTIMIZED
DIGIT	0.740	0.853	0.853
MOUSE-1.3M	10.237	7.064	7.280
MNIST	3.233	3.175	3.196
CIFAR_10	4.369	4.357	4.374
FASHION MNIST	2.989	2.947	2.967
SVHN	4.305	4.283	4.387

KL-divergence value for each dataset apart from the Digit dataset.

4.5 Evaluation of end-to-end performance improvements

For these experiments, we pick the largest dataset - 1.3 million mouse brain cell dataset. We first evaluate the single-thread end-to-end performance of t-SNE implementations.

Table 4: Performance comparison of single threaded runs of various implementations. Dataset used: 1.3 million mouse brain cell dataset. First column and second column mention the implementation name and the execution time in seconds, respectively. The last column presents speedup of an implementation over Sklearn.

IMPLEMENTATION	EXECUTION TIME (s)	SPEEDUP
SKLEARN	28818	1.0×
MULTICORE	15973	1.8×
FlT-SNE	3077	9.4×
DAAL4PY	7684	3.8×
ACC-T-SNE	3125	9.2×

After that, we evaluate the scaling performance of these implementation by increasing number of cores.

4.5.1 End-to-end single thread performance. Table 4 shows the single-thread performance of various t-SNE implementations on 1.3 million mouse cell dataset. Flt-SNE has the fastest single-threaded implementation, with Acc-t-SNE being a close second. However, Acc-t-SNE is 2.5× faster than the second fastest BH t-SNE implementation from daal4py.

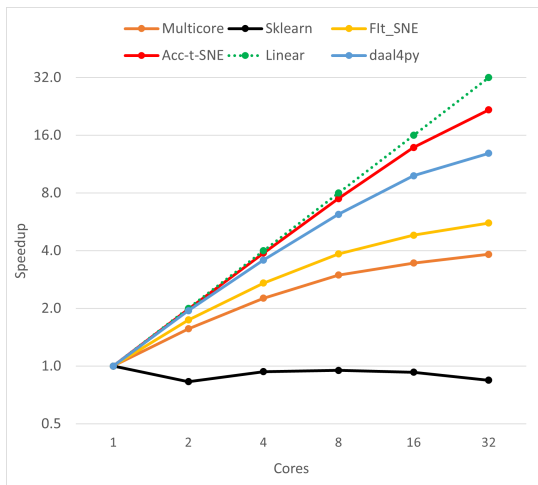


Figure 5: Scaling of various implementations with respect to the number of cores on the mouse brain cell data. The dotted line represents linear scaling. Each solid line presents the scaling of one of the implementations. The points in each solid line show the speedup of the corresponding implementation with respect to its own single-thread execution.

Table 5: Performance comparison on a single thread of daal4py and Acc-t-SNE for each step. Dataset used: 1 million cells subsampled from mouse cell dataset. The first column mentions the step name, second and third columns present the runtime in seconds for each step. The last column presents the speedup of Acc-t-SNE over daal4py for each step.

STEP	DAAL4PY TIME (s)	ACC-T-SNE TIME (s)	SPEEDUP
BSP	12.4	12.2	1.0×
TREE BUILDING	174.4	39.0	4.5×
SUMMARIZATION	29.3	5.6	5.3×
ATTRACTIVE	1226.0	568.5	2.2×
REPULSIVE	3016.3	501.6	6.0×
TOTAL TIME	5391.8	2048.1	2.6×

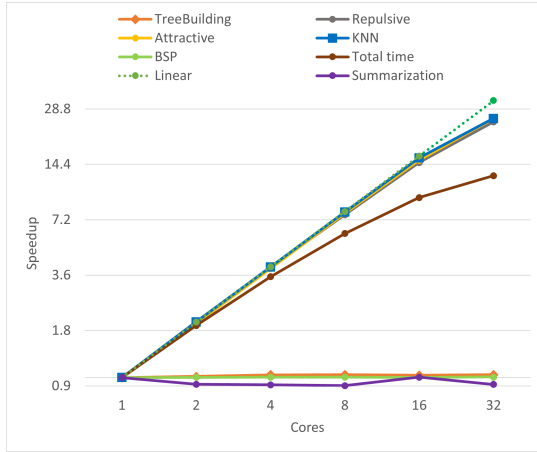
4.5.2 End-to-end multicore scaling. Figure 5 presents the end-to-end multicore scaling of various implementations of t-SNE for the 1.3 million mouse brain cell dataset. Acc-t-SNE scales better than all the other implementations. It achieves the best speedup of 22× when using 32 cores with respect to the single-core performance. Clearly, the improvements in Acc-t-SNE help it scale better than other implementations. This is the scaling of end-to-end execution time. Different steps may scale differently and may have seen different improvements in multicore scaling. In the next section, we will dive deeper into how the improvements help scale individual steps better. As we observed in the previous section, Flt-SNE does well on a single thread but scales poorly to multiple cores. If it could scale well then it can close the gap with Acc-t-SNE.

4.6 Evaluating performance improvements of individual steps

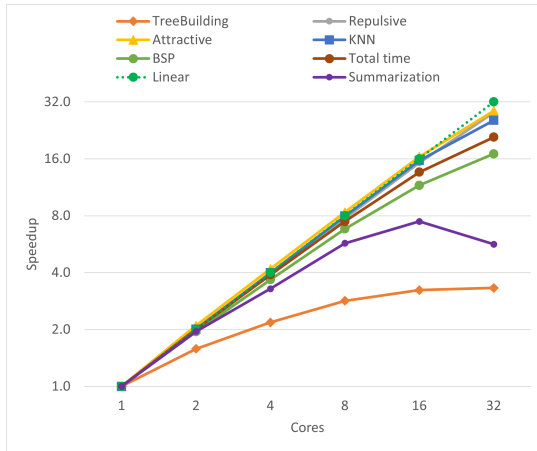
This section presents the performance improvements of Acc-t-SNE for individual steps. For these experiments, for the sake of brevity, we present the results using a single dataset: 1 million cells sampled from mouse-brain cell dataset. We pick daal4py for comparison since it is the fastest implementation prior to our work. First, we present the performance improvements of Acc-t-SNE over daal4py on a single thread. Subsequently, we present our improved scaling. As mentioned in Section 3, the KNN implementation in daal4py is efficient and scales well. We have just used the KNN from daal4py in Acc-t-SNE.

4.6.1 Single thread performance. Table 5 demonstrates that we achieve 2.2–6× speedup over daal4py for individual steps, leading to 2.6× reduction in total time. This performance improvement is a result of 1) efficient Morton-code based

algorithm in Quadtree building, 2) vectorization and software prefetching in the Attractive force step, 3) improvement in data locality and tree traversal by changing the data layout of the tree in Summarization and Repulsive force step. We have not made any single thread performance improvement in BSP since the percentage of time spent in that step is already very small.



(a) Scaling of steps in daal4py.



(b) Scaling of steps in Acc-t-SNE .

Figure 6: Scaling of daal4py and Acc-t-SNE for each step. Dataset used: 1 million cells subsampled from mouse-brain cell dataset. The dotted line represents linear scaling. Each solid line presents the scaling of one of the steps. The points in each solid line present the speedup of the corresponding step with respect to its own single thread execution.

4.6.2 Multicore scaling. The results on multicore scaling of individual steps are presented in Figure 6. Acc-t-SNE shows significant improvements in multicore scaling of various

Table 6: Performance comparison on entire 32 cores of daal4py and Acc-t-SNE for each step. Dataset used: 1 million cells subsampled from mouse cell dataset. The first column mentions the step name, second a third columns present the runtime in seconds for each step. The last column presents the speedup of Acc-t-SNE over daal4py for each step.

STEP	DAAL4PY TIME (s)	ACC-T-SNE TIME (s)	SPEEDUP
BSP	12.3	0.7	17×
TREE BUILDING	168.3	11.7	14.3×
SUMMARIZATION	31.9	1.0	32.4×
ATTRACTIVE	48.0	19.8	2.4×
REPULSIVE	123.0	17.8	6.9×
TOTAL TIME	431.1	98.3	4.4×

steps. These improvements provide additional performance gains over the speedups obtained on a single core. Note the following about the speedup of 32 cores over a single core for each step for both implementations:

- The speedup of Attractive step increases from 24× for daal4py to 28.7× for Acc-t-SNE .
- The speedup of Repulsive step increases from 26.8× for daal4py to 28.1× for Acc-t-SNE .
- The speedup of Summarization step increases from 1.1× for daal4py to 5.7× for Acc-t-SNE .
- Daal4py gets no speedup for Summarization, Quadtree building, and BSP since these steps are single threaded. On the other hand, Acc-t-SNE achieves 5.7× speedup for Summarization, 3.3× for Quadtree building and 17× speedup for BSP.

4.6.3 Multicore performance. Table 6 demonstrates the combined effect of single thread improvements and multicore scaling improvements done in Acc-t-SNE . We achieve 2.4 – 32.4× speedup over daal4py for individual steps, leading to 4.4× reduction in the total time. Considering that Attractive and Repulsive were the primary steps in the single threaded execution of daal4py, the performance improvements in those steps have certainly helped. However, the 14.3× speedup achieved for Quadtree building is quite significant since, with Attractive and Repulsive steps achieving good multicore scaling, the Quadtree step becomes the most time consuming step of daal4py in the 32-core execution. The performance improvements of BSP and Summarization steps are also significant. Otherwise, with the performance improvements in other steps, they would have become bottlenecks.

5 CONCLUSION

Efficient implementations of machine learning algorithms enable researchers to conduct large-scale experiments. In this work, we have implemented an accelerated version (Acc-t-SNE) of the t-SNE algorithm for modern multi-core CPUs. We employed several improvements of single-thread performance and multithread scaling to a majority of steps of BH t-SNE and implemented parallel versions of the previously sequential steps. Acc-t-SNE provides superior single-thread performance and multi-core scaling compared to the state-of-the-art BH t-SNE implementations. To the best of our knowledge, it is the fastest implementation of t-SNE on CPUs providing upto 4× speedup over previous state-of-the-art.

REFERENCES

- [1] 10x Genomics. 2017. Transcriptional Profiling of 1.3 Million Brain Cells with the Chromium Single Cell 3'Solution. (2017).
- [2] Josh Barnes and Piet Hut. 1986. A hierarchical O (N log N) force-calculation algorithm. *nature* 324, 6096 (1986), 446–449.
- [3] Martin Burtscher and Keshav Pingali. 2011. An efficient CUDA implementation of the tree-based Barnes-Hut n-body algorithm. In *GPU computing Gems Emerald edition*. Elsevier, 75–92.
- [4] AWS EC2 C6i. Accessed: October 2022. Amazon EC2 C6i Instances. <https://aws.amazon.com/ec2/instance-types/c6i/>.
- [5] David M Chan, Roshan Rao, Forrest Huang, and John F Canny. 2018. t-SNE-CUDA: GPU-Accelerated t-SNE and its Applications to Modern Data. In *2018 30th International Symposium on Computer Architecture and High Performance Computing (SBAC-PAD)*. IEEE, 330–338.
- [6] David M Chan, Roshan Rao, Forrest Huang, and John F Canny. 2019. GPU accelerated t-distributed stochastic neighbor embedding. *J. Parallel and Distrib. Comput.* 131 (2019), 1–13.
- [7] Intel daal4py. Released: April 2022. daal4py - A Convenient Python API to the Intel(R) oneAPI Data Analytics Library. <https://pypi.org/project/daal4py/>.
- [8] Li Deng. 2012. The mnist database of handwritten digit images for machine learning research. *IEEE Signal Processing Magazine* 29, 6 (2012), 141–142.
- [9] Geoffrey E Hinton and Sam Roweis. 2002. Stochastic neighbor embedding. *Advances in neural information processing systems* 15 (2002).
- [10] Alex Krizhevsky, Geoffrey Hinton, et al. 2009. Learning multiple layers of features from tiny images. (2009).
- [11] Siu Kwan Lam, Antoine Pitrou, and Stanley Seibert. 2015. Numba: A LLVM-Based Python JIT Compiler. In *Proceedings of the Second Workshop on the LLVM Compiler Infrastructure in HPC (Austin, Texas) (LLVM '15)*. Association for Computing Machinery, New York, NY, USA, Article 7, 6 pages. <https://doi.org/10.1145/2833157.2833162>
- [12] Christian Lauterbach, Michael Garland, Shubhabrata Sengupta, David Luebke, and Dinesh Manocha. 2009. Fast BVH construction on GPUs. In *Computer Graphics Forum*, Vol. 28. Wiley Online Library, 375–384.
- [13] George C Linderman, Manas Rachh, Jeremy G Hoskins, Stefan Steinerberger, and Yuval Kluger. 2019. Fast interpolation-based t-SNE for improved visualization of single-cell RNA-seq data. *Nature methods* 16, 3 (2019), 243–245.
- [14] Leland McInnes, John Healy, and James Melville. 2018. Umap: Uniform manifold approximation and projection for dimension reduction. *arXiv preprint arXiv:1802.03426* (2018).
- [15] Guy M Morton. 1966. A computer oriented geodetic data base and a new technique in file sequencing. (1966).
- [16] Yuval Netzer, Tao Wang, Adam Coates, Alessandro Bissacco, Bo Wu, and Andrew Y Ng. 2011. Reading digits in natural images with unsupervised feature learning. (2011).
- [17] Corey Nolet, Avantika Lal, Rajesh Ilango, Taurean Dyer, Rajiv Movva, John Zedlewski, and Johnny Israeli. 2022. Accelerating single-cell genomic analysis with GPUs. *bioRxiv* (2022).
- [18] F. Pedregosa, G. Varoquaux, A. Gramfort, V. Michel, B. Thirion, O. Grisel, M. Blondel, P. Prettenhofer, R. Weiss, V. Dubourg, J. Vanderplas, A. Passos, D. Cournapeau, M. Brucher, M. Perrot, and E. Duchesnay. 2011. Scikit-learn: Machine Learning in Python. *Journal of Machine Learning Research* 12 (2011), 2825–2830.
- [19] Dmitry Ulyanov. 2016. Multicore-TSNE. <https://github.com/DmitryUlyanov/Multicore-TSNE>.
- [20] Laurens Van Der Maaten. 2014. Accelerating t-SNE using tree-based algorithms. *The Journal of Machine Learning Research* 15, 1 (2014), 3221–3245.
- [21] Laurens Van der Maaten and Geoffrey Hinton. 2008. Visualizing data using t-SNE. *Journal of machine learning research* 9, 11 (2008).
- [22] Peter van Oosterom and Tom Vijlbrief. 1996. The spatial location code. In *Proceedings of the 7th international symposium on spatial data handling, Delft, The Netherlands*. 12–16.
- [23] Han Xiao, Kashif Rasul, and Roland Vollgraf. 2017. Fashion-mnist: a novel image dataset for benchmarking machine learning algorithms. *arXiv preprint arXiv:1708.07747* (2017).

Optimization Notice: Software and workloads used in performance tests may have been optimized for performance only on Intel microprocessors. Performance tests, such as SYSmark and MobileMark, are measured using specific computer systems, components, software, operations and functions. Any change to any of those factors may cause the results to vary. You should consult other information and performance tests to assist you in fully evaluating your contemplated purchases, including the performance of that product when combined with other products. For more information go to <http://www.intel.com/performance>. Intel, Xeon, and Intel Xeon Phi are trademarks of Intel Corporation in the U.S. and/or other countries.

A SUPPLEMENTAL MATERIAL

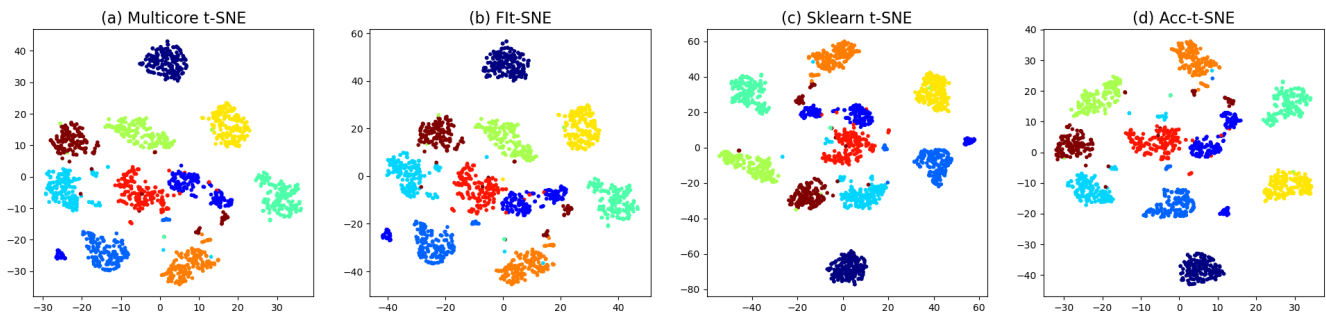


Figure S1: Digits t-SNE plots.

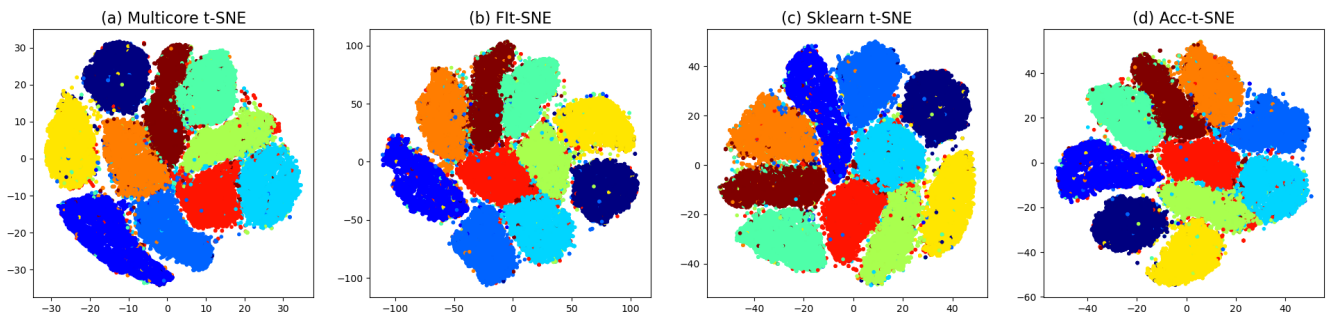


Figure S2: MNIST t-SNE plots.

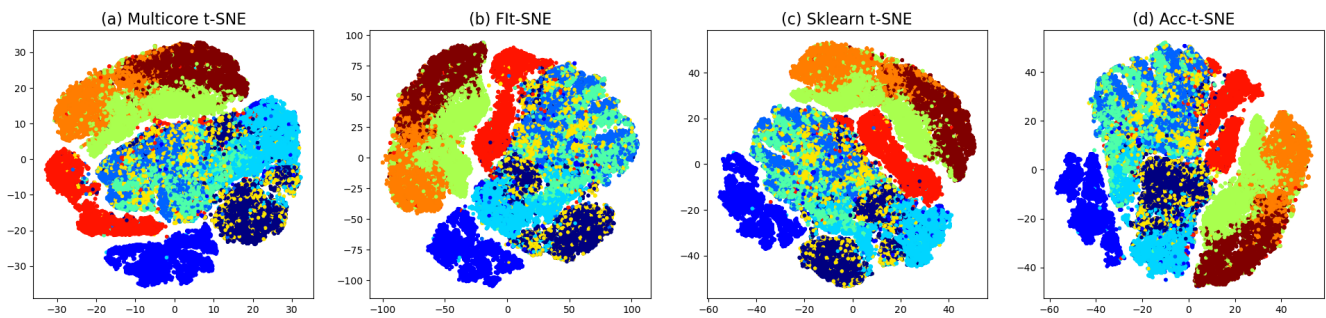


Figure S3: Fashion MNIST t-SNE plots.

Table S1: Acc-t-SNE computation in single-precision (Float32) data format.

DATASET	TIME (s) (FLOAT32)	DIVERGENCE (FLOAT32)	TIME (s) (FLOAT64)	DIVERGENCE (FLOAT64)	SPEEDUP
DIGIT	0.4	0.857	0.4	0.853	0.99×
MOUSE-1.3M	100	7.261	144	7.280	1.4×
MNIST	6.4	3.196	9.0	3.196	1.4×
CIFAR_10	11.7	4.375	19.0	4.374	1.6×
FASHION MNIST	6.3	2.967	9.1	2.967	1.4×
SVHN	26.0	4.386	42.7	4.387	1.6×

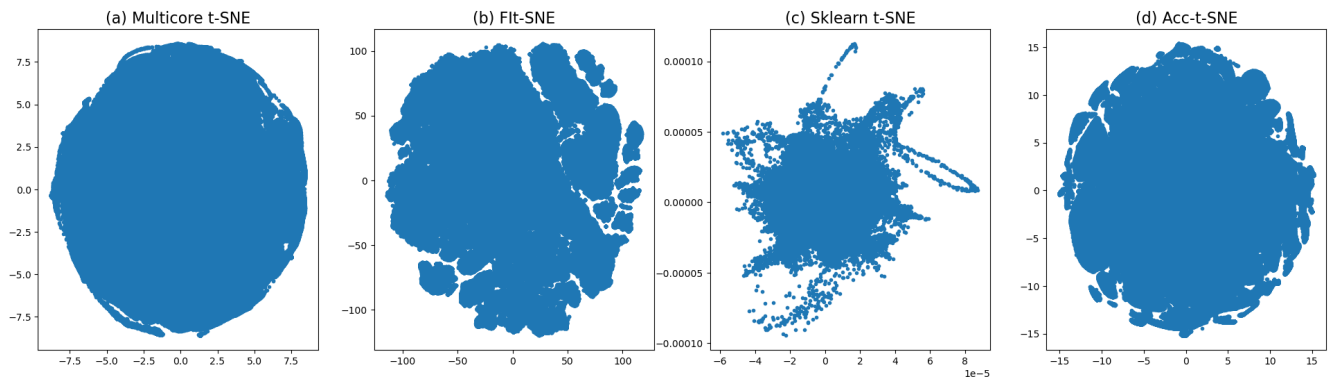


Figure S4: 1.3 million mouse-brain cell t-SNE plots.

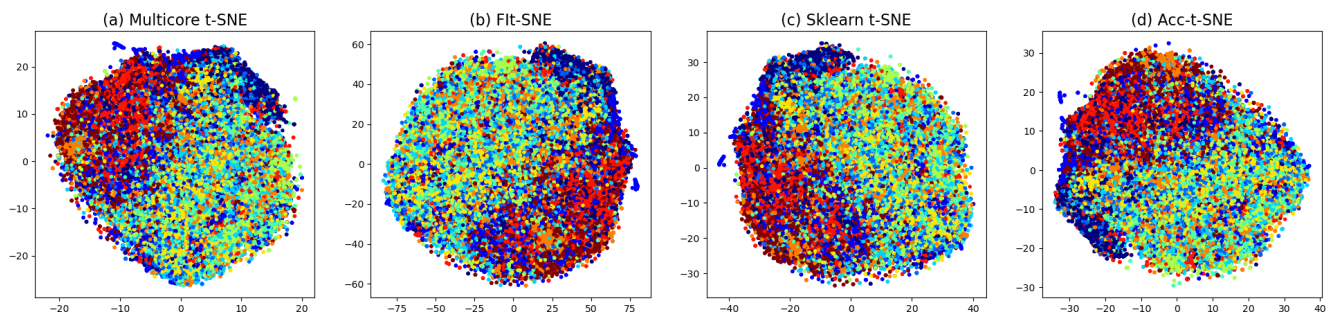


Figure S5: CIFAR-10 t-SNE plots.

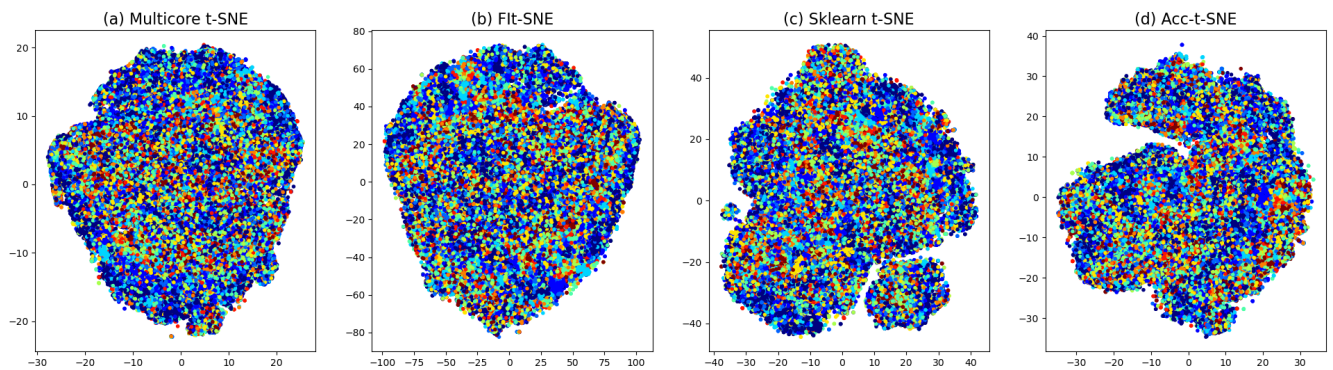


Figure S6: SVHN t-SNE plots.